Solar control of sodium escape from Io

Cesare Grava, Nicholas M. Schneider, François Leblanc, Jeffrey P. Morgenthaler, Valeria Mangano, Cesare Barbieri

AGU PUBLICATIONS

JGR

Journal of Geophysical Research: Planets

RESEARCH ARTICLE
10.1002/2013JE004504

Key Points:
- A spectroscopic study of Io' sodium neutral cloud is performed
- We observe a decrease in Io sodium neutral cloud density after Jupiter eclipse
- Interruption of photodissociation of NaCl can cause the observed decrease

Correspondence to:
C. Grava,
cgrava@swri.edu

Citation:
Grava, C., N. M. Schneider, F. Leblanc, J. P. Morgenthaler, V. Mangano, and C. Barbieri (2014), Solar control of sodium escape from Io, *J. Geophys. Res. Planets*, *119*, 404–415, doi:10.1002/2013JE004504.

Received 18 AUG 2013
Accepted 28 JAN 2014
Accepted article online 4 FEB 2014
Published online 4 MAR 2014

Solar control of sodium escape from Io

Cesare Grava[1,2,3], Nicholas M. Schneider[2], François Leblanc[4], Jeffrey P. Morgenthaler[5], Valeria Mangano[6], and Cesare Barbieri[3]

[1]Southwest Research Institute, San Antonio, TX, USA, [2]LASP, University of Colorado, Boulder, CO, USA, [3]Dipartmento di Astronomia, Università degli Studi di Padova, Padua, Italy, [4]LATMOS/IPSL, Université Pierre et Marie Curie, CNRS, Paris, France, [5]Planetary Science Institute, Fort Kent, ME, USA, [6]IAPS/INAF, Rome, Italy

Abstract We report ground-based spectroscopic observations of the Io sodium cloud before and after eclipse by Jupiter, in a search for possible effects of sunlight on the total atomic sodium content in Io's exosphere. These observations test the importance of the Sun in maintaining the supply of atoms from the thicker atmosphere, which lies close to the surface, to the thinner, more extended, sodium cloud. We performed ground-based spectroscopy of the sodium doublet at 589 nm with a high-resolution échelle spectrograph on the Italian National Telescope Galileo on La Palma Island. We find that the total atomic sodium content immediately after eclipse falls by a factor of ~4 during eclipse and recovers to preeclipse values on a timescale of ~5 h. We evaluate potential causes of the precipitous drop including condensation of the atmosphere, collapse of the ionosphere, and changes in atmospheric chemistry. We conclude that most plausible cause of the drop in atomic sodium production is the interruption of photodissociation of sodium-bearing molecules during eclipse. We discuss further implications of this change in atmospheric chemistry.

1. Introduction

Io possesses one of the most astonishing atmospheres of the solar system. It comes ultimately from the intense volcanic activity caused by tidal heating between Jupiter and Europa and Ganymede and is responsible for both the creation of the plasma torus that encircles Jupiter at Io's orbit and the coupling between the ionospheres of Io and Jupiter [*Bonfond et al*., 2012; *Yoneda et al*., 2013].

Io's atmosphere was indirectly discovered by a Pioneer 10 S band radio occultation experiment, which detected the presence of an ionosphere at Io from 60 to 140 km of altitude [*Kliore et al*., 1974]. The radio occultation experiment was repeated some 20 years later with Galileo spacecraft, confirming the existence of a bound ionosphere within a few hundred kilometers of Io's surface [*Hinson et al*., 1998]. The very same year of the discovery of Io's ionosphere, sodium was detected at Io [*Brown*, 1974], and *Trafton et al*. [1974] soon found it to come from an extended neutral cloud and not from Io itself. *Bergstralh et al*. [1975] demonstrated that the mechanism for exciting this element was resonant scattering of sunlight, which makes the Io sodium cloud brightness remarkably dependent on Io's orbital longitude (see section 3.1 for a description of the resonant scattering mechanism). Further studies showed that the sodium cloud is essentially shaped like a banana extending along Io's orbit and is populated by slowly escaping sodium atoms (~2 km s^{-1} relative to Io). Its morphology is controlled by celestial mechanics and ionization from the plasma torus. Additional escape mechanisms populate other components of the sodium cloud, but they are not part of the present study. These topics are reviewed by, e.g., *McGrath et al*. [2004], *Lellouch et al*. [2007], and by *Schneider and Bagenal* [2007].

The origin of the extended neutral cloud of Io is ultimately its collisionally thick atmosphere, which was first directly observed by Voyager/infrared interferometer spectrometer 7.3 μm spectra, through detection of SO_2 at Loki Patera [*Pearl et al*., 1979]. SO was then discovered [*Lellouch et al*., 1996]. These, plus their dissociation byproducts, are the main constituents of Io's atmosphere. Additional minor percentages are represented by S_2 [*Spencer et al*., 2000], K [*Trafton*, 1975], NaCl [*Lellouch et al*., 2003], and perhaps KCl [*Moullet et al*., 2013].

Although the importance of Io's atmosphere in supplying the plasma torus is well established, it is not yet understood how the atmosphere is maintained. Two different mechanisms were proposed: volcanic outgassing or sublimation of SO_2 frost, but it is not clear which process dominates. Volcanism is thought to be important because of the amount of material outgassed at the vents, but sublimation is also a key process

because of exponential dependence of SO_2 vapor pressure as a function of surface temperature. In the past years there has been evidence for both these processes.

Researchers have attempted to distinguish between the two atmospheric sources by studying the behavior of the atmosphere under different solar illumination conditions. *Retherford et al*. [2007] combined Hubble Space Telescope's (HST) Advanced Camera for Surveys (ACS) and New Horizons' Alice UV spectra to study Io's brightness during eclipses by Jupiter's shadow. They found a decrease of UV brightness of Io's atmosphere that is consistent with a volcanic contribution of just 3% to the overall supply. *Jessup et al*. [2004] found a latitudinal variation (or a dependence on solar zenith angle) of atmospheric column density: SO_2 was seen to peak near the subsolar point, with large column densities (up to 1.8×10^{17} cm^{-2}), and decrease in latitude, as expected for a sublimation-supported atmosphere. *Roth et al*. [2011] found, modeling images from HST/ACS and New Horizons' Long Range Reconnaissance Imager of Io aurora, a decrease in the column density (OI, SI, Na, and K) after eclipse of ~10%. And *Trafton et al*. [2012] showed spectra from HST's Space Telescope Imaging Spectrograph which are consistent with a partial atmospheric collapse (SO_2 and SO) during the eclipse.

In favor of the volcanically driven atmosphere, *Feaga et al*. [2009] found that the atmospheric distribution appears to be best correlated with the location of hot spots and known volcanic plumes. Moreover, no variation of SO_2 column density was seen with varying heliocentric distance, as one would expect for a sublimation-driven atmosphere. More recently, *Spencer et al*. [2012] analyzed HST's Cosmic Origins Spectrograph UV spectra of Io just before and after egress from Jupiter's shadow and compared them with a model of equilibrium sublimation of SO_2 column abundance as a function of time (and thus of surface temperature). The spectra showed an increase of brightness after emergence from eclipse much smaller than predicted. This would be consistent with a volcanically driven atmosphere. The observations, then, offer no clear consensus on whether volcanic outgassing or sublimation dominates the supply to the atmosphere.

Alternatively, the answer could lie in a "hybrid" atmosphere. *Tsang et al*. [2012, 2013] have found that the anti-Jovian atmosphere has a large sublimation-supported component. Taking this together with the results of *Spencer et al*. [2012] on eclipse would suggest that the atmosphere is sublimation dominated on the anti-Jovian hemisphere and volcanically dominated on the Jupiter-facing one.

The possibility of condensation of Io atmosphere during eclipse has long been debated since the discovery, by *Binder and Cruikshank* [1964], of a posteclipse brightening (PEB) of Io's albedo of 0.09 stellar magnitudes in the blue filter. They attributed it to condensation of CH_4 or N_2 that would make Io's surface more reflective at the observed wavelength (Incidentally, this work far predated the actual discovery of Io's atmosphere, 10 years later.). *Fanale et al*. [1981] then attributed a more realistic condensation of the recently discovered SO_2. Its vapor pressure is strongly dependent on the temperature; thus, only at subsolar point (T ~ 130 K, vapor pressure of 1.4×10^{-7} bars), there would be enough frozen SO_2 to produce the brightening. This could explain why other observers did not detect a posteclipse brightening (*Franz and Millis* [1971], *Fallon and Murphy* [1971], *Nelson* [1977], and more recently, *Cruikshank et al*. [2010] with a work in the near IR). Other explanations were proposed, like the correlation of the brightening with solar flares [*Nelson and Hapke*, 1978] or nonuniform distribution of high-blue albedo reflectors at Io's surface (which is redder than any other Galilean satellite and redder in the sub-Jovian point compared to anti-Jovian point), whose dimensions are consistent with large impact craters observed on Moon and Mars [*Frey*, 1975]. But the most plausible explanation remains the condensation. *Nelson et al*. [1993] last summarized the status of PEB detection and nondetections. They found no significant posteclipse brightening between 1981 and 1989 at the 15% level detected by previous observations and concluded that if PEB is indeed real, it must require an additional source of energy (e.g., warming caused by impact of magnetospheric particles), besides solar heating alone (evaporation). Despite the fact that the reality of the PEB is questionable, it was the first phenomenon that hinted to a sublimation-supported atmosphere.

Enhancements of the column density (of different species) in Io's atmosphere after eclipse have been observed in the UV (*Retherford et al*. [2007] and *Wolven et al*. [2001] for OI and SI) and in the infrared (*Bellucci et al*. [2004] for SO_2; interestingly, these authors did not find posteclipse brightening in the visible). The present work is the first one that shows a change in the sodium column density of Io's neutral cloud during Jupiter's eclipse in the visible.

Clarke et al. [1994] showed the possible role that the ionosphere has in supplying atoms to the neutral clouds. They observed a decrease of brightness in the HST's faint object spectrograph FUV spectra of Io in eclipse, which

appears to be consistent with collisional slowing and molecular recombination of photoelectrons if the emissions are ionospheric in nature, as the timescale for decrease of ionospheric electron density appears similar (1000 s) to the timescale for decrease in emission line brightness (~1200 s). In this hypothesis, collisional cooling of photoelectrons is the reason for the degradation in energy. However, the authors proposed an alternative explanation, which involves the decrease of atmospheric column density. This would be the case if the excitation is due to the more energetic torus electrons, which still impact onto Io's atmosphere during eclipse.

The present study seeks to contribute another piece to the puzzle by examining the behavior of escaping sodium during eclipse. The escape rate could be reduced by condensation of the bulk atmosphere, if sublimation dominates. It could also be affected by changes in Io's ionosphere, which in turn affects how the Io plasma torus interacts with Io's atmosphere. Finally, the escape could be affected by atmospheric photochemistry, since the source of atomic Na is thought to be photolysis of volcanically outgassed NaCl [*Moses et al*., 2002; *Lellouch et al*., 2003].

The central method of the present work is to study the response of escaping sodium to the changing solar flux as Io enters and exits eclipse in Jupiter' shadow, by looking at the variation in brightness of its extended, collisionless, sodium neutral cloud. Comparable observations have been reported at conferences [*Anderson et al*., 1999; *Morgan et al*., 2004; *Corliss et al*., 2013], but their results have never been formally published. We will present in section 2 the details of the observations and data reduction. Then we will analyze the calibration from brightness to column density (section 3). In section 4, we will present results and statistical analysis. Section 5 discusses and summarizes the results. Section 6 wraps up the conclusions.

2. Observations and Data Reduction

Our data were taken at the Italian 3.6 m Telescopio Nazionale Galileo (TNG), located on the island of La Palma, with the high-resolution cross-dispersed échelle spectrograph Spettrografo ad Alta Risoluzione Galileo, which covered, simultaneously, the wavelength range between 370 and 1000 nm. We used the long slit (26.7 × 0.40 arc sec), which provided a resolution of 115,000 and a spectral dispersion of 0.022 Å/pixel. The slit was coupled with a filter, conceived for the study of planetary exospheres, which isolates the region of sodium, preventing order overlap otherwise present with the long slit. The slit was placed nearly always parallel to Io's orbital plane, in order to detect the emission of the banana-shaped cloud. The data were binned 2 times in the spatial direction, giving a sampling of 0.33 arc sec/pixel. Standard data reduction includes bias removal, flatfielding, and wavelength calibration, performed using a Thorium-Argon reference lamp. Sporadic cosmic rays interfering with the data reduction process were manually removed.

In order to have an unobstructed view of eclipse ingress and egress, we observed Io before and after Jupiter-Earth conjunction, respectively. Therefore, the four nights (two for each event) were allocated over a 4 month period, from April to July 2007. The geometries of the observations are illustrated in Figure 1

The order-separating narrowband sodium filter introduced interference patterns in the spectra which were removed by a multiparameter numerical fit to the wavelength and spatial dependence, allowing for small wavelength shifts and changes in amplitude.

The seeing was very good, never exceeding 1.6 arc sec full width at half maximum (calculated as a deconvolution of a Gaussian fit to Io's continuum and the theoretical diameter of Io's disk, 1.2 arc sec). Details of observations are summarized in Table 1.

Spectra then must be corrected for spectral signatures of atoms and molecules in the atmosphere of Earth, mostly water, which absorb over narrow bands at many places over our spectral range. To get the spectral profile of the telluric absorptions, we observed several B stars (taken at similar air masses encompassing those of the object to be corrected), whose rapid rotation blurs their intrinsic spectral features. The spectra of these stars present nearly no intrinsic absorption; thus, they will have absorption lines from only Earth's atmosphere. Stars were collapsed to one dimension and then divided into all satellite spectra. Careful attention is required in this step, because stars at slightly wrong air mass will cause either a "negative absorption" (i.e., a false emission) if the air mass is greater than that of the object or an insufficient correction in the opposite case. When there were no good combinations of stars, an artificial star of the desired air mass is created by raising the original stellar spectrum to the power of the ratio of the optical depths (ratio between the desired air mass and the air mass of the star available) and renormalizing. This

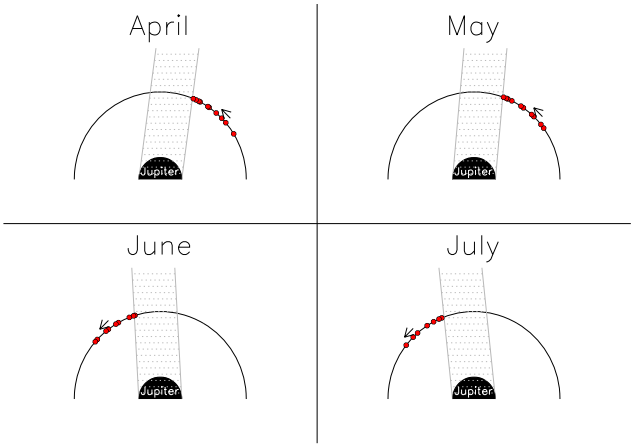

Figure 1. Observations as seen from Earth (at bottom). April and May were preeclipse events, while June and July were posteclipse events. The Earth-Jupiter-Sun angle changes slightly from month to month.

process also creates an additional wavelength (and hence velocity) solution, since all spectra are referenced to the telluric absorptions in Earth's reference frame.

To optimally study the exospheric emission, the reflected sunlight from Io must be removed. This is accomplished using another Jovian satellite as reference (which can be Europa, Ganymede, or Callisto, depending on the right air mass and on the quality of the spectrum). First, the telluric-corrected satellite spectrum is collapsed to one dimension. Then, the satellite is shifted in order to match the Doppler shift of Io, because the

Table 1. Io Parameters; λ_{iii} is the Magnetic Longitude of Io

Spectrum Name	Date Observation (UT)	Orbital Longitude (Deg)	Heliocentric Velocity (km/s)	λ_{III} (Deg)	Air Mass	Brightness (kR)	Integrated Column Density (cm^{-2})
jdei0102	25 Apr 2007 2:07	316	11.62	28	2.04	845	5.75E + 12
jdei0106	25 Apr 2007 3:14	325	9.44	59	1.69	607	4.83E + 12
jdei0109	25 Apr 2007 3:45	330	8.29	73	1.62	577	5.08E + 12
jdei0112	25 Apr 2007 4:20	335	6.96	89	1.58	449	4.95E + 12
jdei0114	25 Apr 2007 4:56	340	5.54	106	1.6	434	6.39E + 12
jdei0115	25 Apr 2007 5:08	342	5.05	112	1.62	317	4.62E + 12
jdei0119	25 Apr 2007 5:47	347	3.44	130	1.73	257	6.02E + 12
jdei0120	25 Apr 2007 5:59	349	2.93	135	1.78	180	4.95E + 12
jdei0121	25 Apr 2007 6:11	350	2.47	140	1.83	51	1.37E + 12
jdei0122	25 Apr 2007 6:14	352	1.96	146	1.9	29	9.64E + 11
jdwf0002	11 May 2007 0:22	316	11.63	212	2.44	442	3.23E + 12
jdwf0004	11 May 2007 0:46	319	10.9	223	2.16	473	3.62E + 12
jdwf0008	11 May 2007 1:29	325	9.45	243	1.84	410	3.62E + 12
jdwf0010	11 May 2007 1:43	327	8.92	249	1.76	386	3.67E + 12
jdwf0015	11 May 2007 2:36	335	6.93	274	1.61	296	3.78E + 12
jdwf0017	11 May 2007 2:52	337	6.3	281	1.59	259	3.80E + 12
jdwf0022	11 May 2007 3:43	344	4.23	305	1.6	162	3.71E + 12
jdwf0024	11 May 2007 3:58	347	3.61	312	1.62	130	3.40E + 12
jdwf0025	11 May 2007 4:10	348	3.11	317	1.64	99	2.82E + 12
jdwf0026	11 May 2007 4:24	350	2.52	324	1.68	55	1.64E + 12
jfqi0034	20 Jun 2007 23:43	10	−3.62	182	1.58	62	9.99E + 11
jfqi0035	20 Jun 2007 23:55	12	−4.13	188	1.57	81	1.12E + 12
jfqi0037	21 Jun 2007 0:11	14	−4.79	195	1.57	110	1.34E + 12
jfqi0043	21 Jun 2007 1:11	23	−7.22	223	1.63	200	1.74E + 12
jfqi0045	21 Jun 2007 1:26	25	−7.76	230	1.67	231	1.87E + 12
jfqi0049	21 Jun 2007 2:05	30	−9.27	248	1.84	273	1.95E + 12
jfqi0051	21 Jun 2007 2:20	33	−9.82	255	1.93	275	1.90E + 12
jfqi0056	21 Jun 2007 3:18	41	−11.8	282	2.57	315	2.00E + 12
jfqi0058	21 Jun 2007 3:34	43	−12.31	289	2.88	330	2.08E + 12
jggv0044	6 Jul 2007 21:59	10	−3.56	7	1.64	30	4.49E + 11
jggv0045	6 Jul 2007 22:11	12	−4.06	13	1.61	48	6.87E + 11
jggv0049	6 Jul 2007 22:42	16	−5.34	27	1.57	83	9.45E + 11
jggv0052	6 Jul 2007 23:12	20	−6.55	41	1.56	120	1.15E + 12
jggv0058	7 Jul 2007 0:08	28	−8.72	67	1.64	210	1.60E + 12
jggv0062	7 Jul 2007 0:42	33	−9.97	82	1.76	266	1.83E + 12
jggv0067	7 Jul 2007 1:26	39	−11.47	103	2.05	265	1.68E + 12

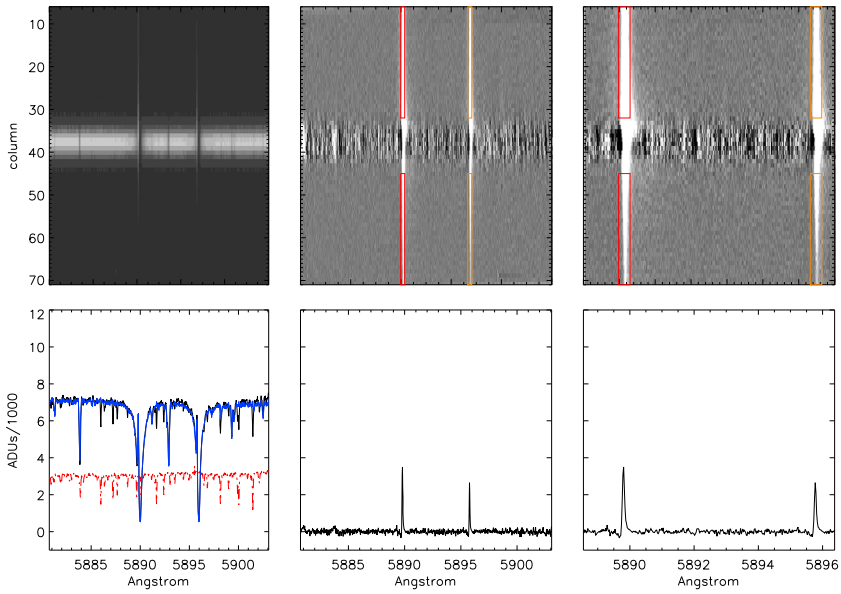

Figure 2. The reduction steps. (top row) Io (left) before and (middle) after continuum removal. (bottom row) Corresponding plots (see text for description). The red and orange boxes correspond to the region around D2 and D1 line, respectively, where we added up signal from Io sodium cloud (see section 3.2). The panels on the top right are zoom of the corresponding middle panels.

different heliocentric velocities of the two objects lead to different positions of the deep Fraunhofer lines. The shift, calculated from the difference of the two predicted heliocentric radial velocities (from Jet Propulsion Laboratory (JPL) Horizons' website), is then adjusted manually to account for small amounts of instrument flexure between exposures. Attention must be paid in the removal of the solar spectrum, because small errors in the shift lead to large features near the bottom of the Fraunhofer lines, which could be mistaken for high-velocity features. We checked the accuracy of the shift by looking at the shape of the solar nickel line at 5892.88 Ц: a mismatch between the solar reflected sunlight of the two satellites would show up in a double-peaked nickel line, one peak in apparent absorption (from Io spectrum) and one in emission (from the subtraction of the satellite). The accuracy is 2 mÅ or 90 m/s. Finally, the satellite spectrum is expanded (i.e., copied to itself) to 2-D, scaled to the value of Io's continuum and then subtracted by the original 2-D Io spectrum.

In Figure 2 we show an example of the reduction steps. The two rightmost frames are just zooms of the corresponding central frames. The top row shows the science frames (left) before and (middle) after the subtraction of the continuum. The two Na emission lines are clearly visible (the *x* axis is the same as the bottom row). In the bottom left graph there are the corresponding plots of Io's continuum along the central column (solid black line), plus the star (normalized to scale at Io's continuum but shifted in the vertical direction for clear visibility), in red dashed line. The blue line is Io's spectrum without telluric lines. The difference between Io and the shifted satellite (both corrected for telluric absorptions) is plotted in the second graph (bottom row), with same *y* axis as the left graph. Only the emission from Io is visible.

For some of the posteclipse spectra, it was necessary to remove a ghost spectrum of Jupiter on top of the science frames, caused by internal reflections within the instrument. This was accomplished using a Jupiter spectrum properly scaled to match its ghost. As a result, these regions suffer from slightly higher noise. For nearly all the spectra, a very small positive background, presumably due to light scattered within the instrument, was also removed manually before performing all these operations.

3. Calibration and Conversion to Column Density

Absolute intensity calibration is performed by comparing the emission spectra to the disk of Jupiter. The center of Jupiter's disk has a well-known surface brightness of 5.6 MegaRayleighs $Å^{-1}$, within 20% [*Brown and Schneider*, 1981; *Bouchez et al*., 2000], so it is straightforward to convert analog-to-digital units (ADUs) in Rayleighs (1 Rayleigh = $10^6/4\pi$ photons s^{-1} cm^2 sr^{-1} [see, e.g., *Brown et al*., 1983]).

3.1. The Resonant Scattering Mechanism

In the resonant scattering mechanism, a solar photon hits a sodium electron that jumps to the first excited state, and when it returns to the ground state (after nearly 10^{-7} s), it emits a photon. The first excited state is in reality split due to the fine structure, so this process can actually emit in two possible wavelengths: 5889.95 and 5895.92 Å for the D2 and D1 line, respectively. For our primary goal of measuring relative column abundances, it was sufficient to assume an optically thin column. Our maximum pixel brightness was 20 kiloRayleighs, corresponding to an optical depth of 0.5 for the D2 line [*Brown and Yung*, 1976, equation (17)] assuming a temperature of 800 K. Furthermore, this small optical thickness correction does not affect the relative brightnesses which are central to this study. In the assumption of an optically thin cloud, the column density is proportional to the brightness through the *g* factor:

$$4\pi E = g \cdot N$$

where *N* is the column density expressed in atoms cm^{-2}, and *E* is the brightness expressed in units of 10^6 photons $cm^{-2}\,s^{-1}\,sr^{-1}$ (and 4πE is thus expressed in Rayleighs).

The *g* factor is expressed in photons $atoms^{-1}\,s^{-1}$ and is the production of the scattering efficiency and the number of available photons, i.e., a measure of the efficiency with which sunlight is scattered by sodium atoms. The complete expression is [*Brown and Yung*, 1976]

$$g = \left[\gamma \cdot \pi F_{\odot} \frac{\lambda^2}{c}\right] \frac{\pi e^2}{mc} f$$

where *e* and *m* are, respectively, the electron charge and mass, *f* is the oscillator strength, πF the solar flux at Io at the sodium wavelength, and *c* the speed of light. The variable γ is defined as the ratio of the solar flux at a given Doppler shift of the sodium atoms (with respect to the Sun) to that of the nearby solar continuum. Thus, γ depends on the heliocentric radial velocity of the sodium, and for sodium comoving with Io, this in turn depends on the orbital longitude of Io. Therefore, even in the case of constant sodium column abundance, the brightness of the sodium cloud changes with the orbital phase of Io. In fact, at maximum elongations (±90°), Io's sodium cloud is brightest because the heliocentric radial velocity is maximum ($\pm 17\ km\,s^{-1}$) and so too γ (~ 0.70). In contrast, at orbital longitudes = 0° and 180° the heliocentric radial velocity is zero and so is the Doppler shift from the bottom of the Fraunhofer line, and γ is minimum (~ 0.05). This means that only 5% of solar flux can be resonantly scattered by sodium atoms, and the cloud is thus much more dimmer and the column density only apparently smaller. The challenge of these observations lies in disentangling this effect from true temporal variations in sodium content. We remove the effect of the changing orbital phase by converting our observations from Rayleighs to column abundances.

We used tabulated values from JPL Horizons website (http://ssd.jpl.nasa.gov/horizons.cgi) to obtain heliocentric radial velocities of Io for the midpoint of each 10 min exposure. Then, we selected a spectral region of ~ 350 mÅ around the peak of Io's exospheric emission, in order to encompass all the light coming from the neutral cloud. We computed the spatial integral of the brightness of the cloud at each wavelength pixel (see section 3.2). For each wavelength pixel, we computed the heliocentric radial velocity as the sum of Io's heliocentric velocity and the Doppler shift of the wavelength pixel (We need to take into account variations in radial velocity along the slit because we found that a shift in ±0.5 km/s leads to a change in the *g* factor which can be as high as 20%). We converted the brightness in each wavelength pixel to column density by dividing by the Doppler-corrected *g* factor.

We used *g* factors interpolated from those tabulated in *Killen et al*. [2009, Figure 7], properly scaled from Mercury's heliocentric distance (to which these are referred) to Jupiter's heliocentric distance. Finally, we summed all these column abundances to get the total column density of the cloud.

3.2. Spatial Profile of the Neutral Cloud

Figure 3 shows a typical exospheric spatial profile for our data set, exhibiting an asymmetric double peak. Previous spatial profiles [e.g., *Schneider et al*., 1991a] exhibit only single peaks at Io's position, attributable to the worse atmospheric seeing of those observations. Such double-peaked profiles are expected for optically thin emissions due to limb brightening, but not for Io, where sodium becomes optically thick below the exobase. This effect was predicted by *Brown et al*. [1975] and *Schneider et al*. [1991a]. The dip in the center of these profiles is probably an artifact of the continuum subtraction, since Io's bright surface at wavelengths

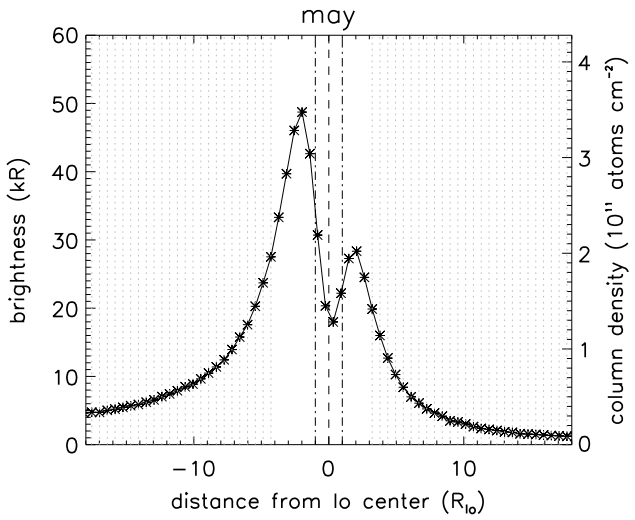

Figure 3. Spatial profile of the brightness of Io's exospheric cloud as a function of position relative to Io's center (asterisks). The dashed lines indicate center of Io's disk; dash-dotted lines indicate ±1.0 R_{Io}. The dotted gray lines indicate the region of coaddition in the spatial direction (i.e., along the slit length).

around the sodium lines is approximately as reflective as an optically thick resonantly scattering cloud. Sodium seen against Io's disk, therefore, has no spectral contrast and leaves no spectral signature. The double peak is therefore the result of the subtraction of the continuum and of the high spatial resolution of the instrument, combined with the low seeing. We therefore avoid the region within the central dip when studying the total cloud abundance. The region where we added up signal consists of ~350 mÅ around the wavelength of Na D lines in Io's reference frame, λ_{Na}^{Io}. This region is not symmetric around λ_{Na}^{Io}, because we want to encompass all emissions from the neutral cloud, and this emission is more extended in the forward direction ("red" for preeclipse months and "blue" for posteclipse months). Such region of integration is indicated in orange and red boxes in Figure 2. The high spatial resolution of this data set, inferred from the double peak and the asymmetry, has motivated a separate study of the spatial structure which will appear in a separate paper.

4. Temporal Behavior

In Figure 4 we show the exospheric column density (averaged from either side of Io) as a function of orbital phase longitudes (increasing counterclockwise and with 0° corresponding to Io in eclipse). Qualitatively, the data exhibit the hypothesized response of the cloud to eclipse: (1) relatively constant behavior before eclipse, (2) an unseen decline during eclipse, and (3) a recovery from low values after eclipse.

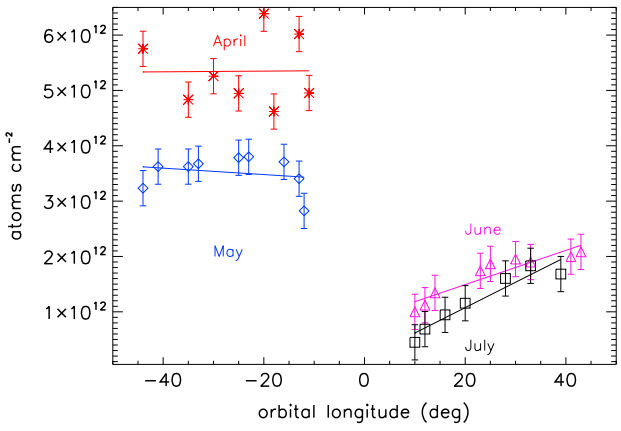

Figure 4. Column density of four nights as a function of orbital longitude. Red asterisks: April; blue diamonds: May; purple triangles: June; black squares: July. Overplotted lines are the linear fit.

Statistical support for this behavior requires error bars on the column abundances, which are challenging to derive from first principles (photon noise and readout noise) given the large number and complexity of reduction steps. We therefore examined the data themselves, to find a reasonable estimate of random errors, attributable to statistical variation in the measurement or to intrinsic stochastic variation of the cloud itself. Of the four data sets in Figure 4, April cannot be

Table 2. Parameters of the Chi-Square Fit to the Data[a]

Month	DOF Const	Chi2 Const	PTE Const (%)	DOF Incr	Chi2 Incr	PTE Incr (%)	*F* Value	PF	Mean	*b*
May	8	1.00	43.35	7	1.09	36.74	0.35	57.26	3.52E + 12	−5.80E + 09 ± 9.40E + 09
June	8	1.62	11.30	7	0.26	97.04	43.60	0.03	1.67E + 12	3.09E + 10 ± 9.25E + 09
July	6	2.78	1.07	5	0.31	90.51	48.11	0.10	1.19E + 12	4.58E + 10 ± 1.18E + 10

[a]The mean is expressed in atoms cm^{-2}, while *b*, the slope, is in atoms cm^{-2} deg^{-1}.

used due to nonphotometric periods during the night (the inferred conversion factor from ADUs to Rayleighs did not behave in a regular way during the night), and we discarded it from our discussion altogether; June and July exhibit systematic trends that exceed any random variations. We therefore selected May to characterize the error bars, adopting their variance about the mean to derive 1-σ errors. The fact that a small systematic trend is visible argues that these error bars may be slightly overestimated. But they are sufficient for chi-square testing for the significance of differences and trends, especially between May, June, and July. Here and in the remainder of the paper, σ is the standard deviation of the points in May: $\sigma = 3.18 \times 10^{11}$ cm^{-2}.

First, we test the hypothesis that the data are adequately fit by a constant value for each month (the mean). May shows a reduced chi-square of unity (by definition) and PTE (probability to exceed, calculated using Interactive Data Language (IDL) routine *chisqr_pdf.pro*) value near 50%, as expected since its variance was used to find the error bars. June and July show reduced chi-square values greater than 1.5, indicating that a constant is a poor fit at 88% and 99% confidence for June and July, respectively. We then add a linear term to the fit. The two posteclipse months' data sets pass the *F* test for the addition of a linear term, at confidence levels of 99.97% (June) and 99.9% (July), respectively. The fractional change in abundance for May was only −8%. May's variation was therefore very small compared to the posteclipse months. The chi-square fit parameters are listed in Table 2. DOF is the number of degrees of freedom; in our case, it is *N* (the number of observations) minus the number of constraints, which is 1 in the first case (data compared to their mean) and 2 in the second case (linear fit); χ^2_ν is the reduced chi-square; *F* is a statistic (adimensional) that follows the *F* distribution and is a measure of how much the additional term has improved the value of the reduced chi-square and should be small when the additional term does not significantly improve the fit [*Bevington and Robinson*, 2003]; PF is the probability to exceed for this statistic *F* and is computed using IDL routine *f_pdf.pro*; mean is the average of the data; finally, *b* is the slope, computed fitting the data with a linear function $y = a + b*x$ where *x* are our orbital longitudes and *y* are our brightnesses.

Next we evaluate the statistical significance of the decline in column abundance during eclipse. The decline, expressed as (last point in May to first point after eclipse)/σ is 5.73 for June and 7.46 for July. This assesses the robustness of our results.

Finally, we examine the behavior after eclipse reemergence. Figure 4 shows that June and July data recovers approximately halfway toward preeclipse values during the ~5 h span of observation. We cannot calculate the recovery timescale without observations reaching the unperturbed value; therefore, we can place a lower limit for the recovery of 5 h.

The data, both statistically and visually, are therefore consistent with relatively constant values before eclipse, a substantial decline during eclipse, and a rapid recovery afterward. In the next section we discuss the implications of this result.

We close this section with a discussion of the robustness of the results and the underlying assumptions. Most notably, it bears repeating that the experiment as a whole requires the sodium cloud to behave similarly at monthly intervals [*Burger et al.*, 2001], meaning that intrinsic variability caused by volcanoes, the magnetosphere, or other unknown causes are small compared to the variability caused by eclipse. The similarity of the drops during eclipse and rapid recoveries after argue against intrinsic variability occurring coincidentally during eclipse.

5. Discussion and Conclusion

Potential causes for the precipitous drop in sodium escape during eclipse can be traced to fundamental solar influences on phase changes, ionization state, and molecular/atomic state in the atmosphere. These can

affect processes which convey sodium from Io's surface or interior to the exosphere. We can identify the dominant influence by (1) evaluating the plausibility of strong dependence on sunlight and (2) determining whether the solar influence has the right magnitude and timescale to match the observed change. Note that the time to populate the inner half of the spectrograph slit length is ~2.5 h at 2 km/s, so a solar influence on this timescale or longer will produce a variation in the cloud on the observed ~5 h timescale.

Sodium presumably begins in molecular form with volcanic outgassing, as evidenced by the detection of NaCl apparently associated with volcanic vents [*Lellouch et al*., 2003; *Moullet et al*., 2010]. From there, NaCl can condense into solid form on the surface and later be ejected in atomic or molecular form by sputtering. Alternatively, NaCl can remain in the atmosphere, eventually be dissociated by sunlight or electrons. Sodium in either atomic or molecular form could be ionized and become an important chemical species in the ionosphere [*Summers and Strobel*, 1996]. On reaching the exosphere, the atomic sodium could be ejected by atmospheric sputtering. Each link in the various chains above has the potential for control by sunlight. Below we evaluate the leading candidates.

5.1. Condensation

An obvious potential cause for the drop in atmospheric escape is the freeze out of the SO_2 atmosphere. Condensation of Io's atmosphere was suggested even before the first detection of the atmosphere, based on apparent brightening of the surface at optical wavelengths on emergence from eclipse. But later attempts to reproduce the original discovery with improved instrumentation failed to do so [*Nelson et al*., 1993], leading to the conclusion that the amount of atmosphere condensing was insufficient to make a highly scattering frost. The presence of a noncondensing gas [*Kumar and Hunten*, 1982; *Kumar*, 1985; *Moore et al*., 2009] or of a steady supply of volcanic gas could prevent significant loss of atmosphere due to condensation.

The effect of SO_2 atmospheric condensation on sodium escape is unclear. If the entire atmosphere and exosphere were to freeze out on the surface, atmospheric sputtering of Na-bearing molecules would cease due to burial of condensed SO_2. But this much condensation is unrealistic, especially given the lack of posteclipse brightening. It is more plausible that the exosphere and the region that supplies it will not condense, and therefore be available for atmospheric sputtering. Even in the limit of complete freeze out, atmospheric sputtering would give way to surface sputtering, reducing yields only slightly [*Johnson*, 1994].

Moreover, the expected timescale for return to preeclipse conditions is ~2 h [*Walker et al*., 2012], which is substantially smaller than our inferred lower limit of 5 h.

In summary, condensation does not meet neither the second requirement of an appropriate timescale for variation nor the first requirement for plausibility of controlling escape.

5.2. Collapse of the Ionosphere

A second explanation for the temporal behavior of our data could be the decline of the ionosphere as Io moves into Jupiter's shadow. There are two potential ionosphere creation processes: photoionization and electron impact ionization. If photoionization dominates, then eclipse will lead to a decline in ionospheric density, and egress will lead to an increase. Theoretical studies [e.g., *Saur et al*., 1999] found that photoionization in a pure SO_2 atmosphere plays a minor role in comparison to collisional ionization and cannot reproduce the observed plasma measurements from Galileo spacecraft [*Frank et al*., 1996]. The potential influence of the ionosphere on sodium escape is also unclear. Sodium molecular ions are recognized as critical for the escape of the high-speed sodium which populates the very extended sodium nebula [*Wilson et al*., 2002]. *Yoneda et al*. [2009] attributed the nebula's brightness variations with Io's orbital phase to ionospheric variations, concluding that Io's ionosphere is controlled by solar radiation in a manner similar to the Earth's. The same logic does not apply to the escape of slow sodium, however, as there is no established process involving the ionosphere. Furthermore, even in a photoionization-dominated ionosphere, the time for ionospheric collapse is too long. Atomic sodium is expected to be the terminal ion in the ionosphere [*Wong and Smyth*, 2000], and the timescale for atomic recombination is measured in thousands of years, not hours [*Summers and Strobel*, 1996, Table II, reaction (R59)].

In summary, ionospheric collapse appears to meet neither requirement for explaining the observed variation. The timescale for recovery in sunlight greatly exceeds the observed value, and there is no known mechanism for the ionosphere to control the escape of slow sodium.

5.3. Photodissociation of NaCl

The third and final potential cause for the drop in atomic sodium escape in eclipse is the interruption of photodissociation of sodium-bearing molecules. These are responsible for the fast components of the neutral cloud, namely, (a) the "stream" or "spray" [*Schneider et al*., 1991b], which appears as fast sodium preceding Io in its orbital plane and almost completely encircling Jupiter and (b) the "jet" or "directional feature" [*Wilson and Schneider*, 1999], which is a narrow emission of sodium very close to Io, aligned in the anti-Jupiter direction. These features, so different in shape, both share the same source: a sodium-bearing molecular ion (NaX^+, where X has for long time been unknown). Some of the most popular photochemical models of the 90's considered compounds of Na with S, O, and Na itself [*Johnson*, 1994; *Summers and Strobel*, 1996] to study NaX. Finally, *Kueppers and Schneider* [2000] detected the ion of chlorine, which sparkled the modeling of NaCl [*Fegley and Zolotov* 2000; *Schaefer and Fegley*, 2005]. NaCl was later confirmed spectroscopically by *Lellouch et al*. [2003] and is now the preferred candidate for such molecular sodium ions.

The most comprehensive NaCl photochemical model to date is the one of *Moses et al*. [2002]. In it, volcanically supplied NaCl undergoes two loss processes: photodissociation (52% of the loss) and condensation via dust onto the surface (48% of the loss). The main loss process for NaCl is also the main source process for atomic Na; indeed, photodissociation accounts for virtually all Na production. Two findings of this model are relevant for our work: (1) more Na is created during the day than during the night (a consequence of the photodestruction of NaCl, see their Figure 10a) and (2) the photochemical lifetime of NaCl is ~3.5 h (Moses' Table A1, reaction (R50)), comparable to our observed timescale for recovery after eclipse. It is not clear whether NaCl is ejected into the cloud and later photodissociated or builds up in the atmosphere, dissociates, and escapes. While the data presented here do contain spatial information, the simultaneous changes in photochemistry, escape processes, and viewing geometry necessitate the development of a detailed numerical model beyond the scope of this paper.

In summary, the interruption of photodissociation meets both requirements for explaining the observed variation: atmospheric modeling shows that photodissociation is the last step in producing atomic sodium which can escape, and the timescales for decline and recovery match those observed.

6. Conclusions

The precipitous drop in escaping sodium atoms during eclipse and the recovery afterward is best explained by the interruption of photodissociation of NaCl while in Jupiter's shadow. We briefly discussed three possible causes for this behavior, two of which are unlikely. The condensation of SO_2 atmosphere is probably not enough to prevent Na-bearing molecules to be surface sputtered: NaCl, the most obvious candidate, is in dynamical equilibrium with volcanic sources, photolysis, and condensation as it hits the ground [*Lellouch et al*., 2003]. Second, the role of photoionization or ionospheric processes, in general, appears to be negligible in affecting escape.

The evidence for the importance of photodissociation has bearing on the behavior of the atmosphere as a whole. *Moses et al*. [2002] show that the primary atmospheric species, SO_2 and its byproducts, are all affected by photodissociation on the short timescales comparable to NaCl. The atomic/molecular mix of escaping particles and the upper atmosphere itself may change during eclipse. Furthermore, the significant response of Io's atmosphere to the "impulse" of eclipse by Jupiter leads us to conclude that photodissociation variations on diurnal timescales will also be important. Escape from Io's dayside is likely to be depleted in molecular species, while nightside escape will be depleted in atomic species. This in turn could lead to asymmetries in escape when Io lies on opposite sides of Jupiter, with different hemispheres facing the Sun and facing into the plasma flow.

These results call for several future observational and modeling efforts. First and foremost, confirming observations, beyond the two cases here, are essential. Second, the development of a time-variable sodium cloud model will be required for comparison with the temporally and spatially resolved eclipse data presented here. Finally, the broad repercussions on atomic versus molecular escape versus orbital longitude should be investigated. The results can be compared to sodium images and spectra and then applied to the major species for which such observations are not yet possible.

Acknowledgments
The authors wish to thank K.D. Retherford, L. Roth, and Joachim Saur for useful discussions on section 5. This work has been supported by NSF's Planetary Astronomy Program, INAF/TNG, and the Astronomy Department and CISAS of University of Padua, through a contract by the Italian Space Agency ASI. The authors also wish to thank Emmanuel Lellouch and another anonymous referee for insightful suggestions during the revision process.

References

Anderson, C. M., J. Corliss, F. Scherb, and A. Potter (1999), Eclipse egress growth of the Na I column density in the vicinity of Io, *Bull. Astron. Soc.*, *31*(4), 1165, #58.06.

Bellucci, G., et al. (2004), Cassini/VIMS observation of an Io post-eclipse brightening event, *Icarus*, *172*, 141–148, doi:10.1016/j.icarus.2004.05.012.

Bergstralh, J. T., D. L. Matson, and T. V. Johnson (1975), Sodium D-line emission from Io: Synoptic observations from Table Mountain Observatory, *Astrophys. J.*, *195*, L131–L135, doi:10.1086/181727.

Bevington, P. R., and K. D. Robinson (2003), *Data Reduction and Error Analysis for the Physical Sciences*, 3rd ed., McGraw-Hill, Boston, MA.

Binder, A. B., and D. P. Cruikshank (1964), Evidence for an atmosphere on Io, *Icarus*, *3*, 299–305, doi:10.1016/0019-1035(64)90038-7.

Bonfond, B., D. Grodent, J.-C. Gérard, T. Stallard, J. T. Clarke, M. Yoneda, A. Radioti, and J. Gustin (2012), Auroral evidence of Io's control over the magnetosphere of Jupiter, *Geophys. Res. Lett.*, *39*, L01105, doi:10.1029/2011GL050253.

Bouchez, A. H., M. E. Brown, and N. M. Schneider (2000), Eclipse spectroscopy of Io's atmosphere, *Icarus*, *148*(1), 316–319, doi:10.1006/icar.2000.6518.

Brown, R. A. (1974), Optical line emission from Io, in "Exploration of the planetary system, in *Proceedings of the Symposium*, vol. 1974, Torun, Poland, September 5-8, 1973" (A75-21276 08-91), pp. 527-531, D. Reidel Publishing Co., Dordrecht.

Brown, R. A., and N. M. Schneider (1981), Sodium remote from Io, *Icarus*, *48*, 519–535, doi:10.1016/0019-1035(81)90061-0.

Brown, R. A., and Y. L. Yung (1976), Io, its atmosphere and optical emissions, in "Jupiter: Studies of the interior, atmosphere, magnetosphere and satellites", in *Proceedings of the Colloquium*, vol. 1976, Tucson, Ariz., May 19-21, 1975, pp. 1102–1145, Univ. Arizona Press, Tucson Discussion, p. 1142.

Brown, R. A., R. M. Goody, F. J. Murcray, and F. H. Chaffee Jr. (1975), Further studies of line emission from Io, *Astrophys. J.*, *200*, L49–L53, doi:10.1086/181894.

Brown, R. A., C. B. Pilcher, and D. F. Strobel (1983), Spectrophotometric studies of the Io torus, in *Physics of the Jovian Magnetosphere*, vol. 1983, pp. 197–225, Cambridge Univ. Press, Cambridge and New York.

Burger, M. H., N. M. Schneider, I. de Pater, M. E. Brown, A. H. Bouchez, L. M. Trafton, Y. Sheffer, E. S. Barker, and A. Mallama (2001), Mutual event observations of Io's sodium corona, *Astrophys. J.*, *563*(2), 1063, doi:10.1086/323944.

Clarke, J. T., J. Ajello, J. Luhmann, N. M. Schneider, and I. Kanik (1994), Hubble Space Telescope UV spectral observations of Io passing into eclipse, *J. Geophys. Res.*, *99*(E4), 8387–8402, doi:10.1029/93JE02547.

Corliss, J. B., W. Harris, A. E. Potter, F. Scherb, F. Roesler, and R. M. Killen (2013), The post-eclipse growth of Io's sodium emissions and a unique glance at the distinct velocity populations of sodium near Io's disk, Magnetospheres of Outer Planets meeting, July 8-12, 2013, Athens, Greece.

Cruikshank, D. P., J. P. Emery, K. A. Kornei, G. Bellucci, and E. D'Aversa (2010), Eclipse reappearances of Io: Time-resolved spectroscopy (1.9–4.2 μm), *Icarus*, *205*, 516–527, doi:10.1016/j.icarus.2009.05.035.

Fallon, F. W., and R. E. Murphy (1971), Absence of post-eclipse brightening of Io and Europa in 1970, *Icarus*, *15*, 492, doi:10.1016/0019-1035(71)90127-8.

Fanale, F. P., W. B. Banerdt, and D. P. Cruikshank (1981), Io: Could SO_2 condensation/sublimation cause the sometimes reported post-eclipse brightening?, *Geophys. Res. Lett.*, *8*(6), 625–628, doi:10.1029/GL008i006p00625.

Feaga, L. M., M. McGrath, and P. D. Feldman (2009), Io's dayside SO_2 atmosphere, *Icarus*, *201*, 570–584, doi:10.1016/j.icarus.2009.01.029.

Fegley, B., and M. Y. Zolotov (2000), Chemistry of sodium, potassium, and chlorine in volcanic gases on Io, *Icarus*, *148*(1), 193–210, doi:10.1006/icar.2000.6490.

Frank, L. A., W. R. Paterson, K. L. Ackerson, V. M. Vasyliunas, F. V. Coroniti, and S. J. Bolton (1996), Plasma observations at Io with the Galileo spacecraft, *Science*, *274*(5286), 394–395, doi:10.1126/science.274.5286.394.

Franz, O. G., and R. L. Millis (1971), A search for an anomalous brightening of Io after eclipse, *Icarus*, *14*, 13, doi:10.1016/0019-1035(71)90097-2.

Frey, H. (1975), Post-eclipse brightening and non-brightening of Io, *Icarus*, *25*, 439–446, doi:10.1016/0019-1035(75)90008-1.

Hinson, D. P., A. J. Kliore, F. M. Flasar, J. D. Twicken, P. J. Schinder, and R. G. Herrera (1998), Galileo radio occultation measurements of Io's ionosphere and plasma wake, *J. Geophys. Res.*, *103*(A12), 29,343–29,358, doi:10.1029/98JA02659.

Jessup, K. L., J. R. Spencer, G. E. Ballester, R. R. Howell, F. Roesler, M. Vigel, and R. Yelle (2004), The atmospheric signature of Io's Prometheus plume and anti-Jovian hemisphere: Evidence for a sublimation atmosphere, *Icarus*, *169*, 197–215, doi:10.1016/j.icarus.2003.11.015.

Johnson, R. E. (1994), Formation of Na-containing molecular ions at Io, *Icarus*, *111*, 65–72, doi:10.1006/icar.1994.1133.

Killen, R. M., D. Shemansky, and N. Mouawad (2009), Expected emissions from Mercury's exospheric species, and their ultraviolet-visible signatures, *Astrophys. J. Suppl.*, *181*, 351–359, doi:10.1088/0067-0049/181/2/351.

Kliore, A., D. L. Cain, G. Fjeldbo, B. L. Seidel, and S. I. Rasool (1974), Preliminary results on the atmospheres of Io and Jupiter from the Pioneer 10 S-band occultation experiment, *Science*, *183*, 323–324, doi:10.1126/science.183.4122.323.

Kueppers, M., and N. M. Schneider (2000), Discovery of chlorine in the Io torus, *Geophys. Res. Lett.*, *27*(4), 513–516, doi:10.1029/199GL01078.

Kumar, S. (1985), The SO_2 atmosphere and ionosphere of Io: Ion chemistry, atmospheric escape, and models corresponding to the Pioneer 10 radio occultation measurements, *Icarus*, *61*, 101–123, doi:10.1016/0019-1035(85)90158-7.

Kumar, S., and D. M. Hunten (1982), The atmosphere of Io and other satellites, in "*Satellites of Jupiter*", pp. 782–806, Univ. of Arizona Press, Tucson, AZ, 1982.

Lellouch, E., D. F. Strobel, M. J. S. Belton, M. E. Summers, G. Paubert, and R. Moreno (1996), Detection of sulfur monoxide in Io's atmosphere, *Astrophys. J. Lett.*, *459*, L107, doi:10.1086/309956.

Lellouch, E., G. Paubert, J. I. Moses, N. M. Schneider, and D. F. Strobel (2003), Volcanically emitted sodium chloride as a source for Io's neutral clouds and plasma torus, *Nature*, *421*, 45–47.

Lellouch, E., M. A. McGrath, and K. L. Jessup (2007), Io's atmosphere, in "*Io After Galileo: A New View of Jupiter's Volcanic Moon*", edited by R. M. C. Lopes and J. R. Spencer. 23 pp., Published by Springer Praxis Books / Geophysical Sciences, Part of Springer Science + Business Media, Berlin, Germany, 2007, doi: 10.1007/978-3-540-48841-5_10.

McGrath, M. A., E. Lellouch, D. F. Strobel, P. D. Feldman, and R. E. Johnson (2004), Satellites atmospheres, in *Jupiter. The Planet, Satellites and Magnetosphere*, Cambridge Planetary Science, vol. 1, edited by F. Bagenal, T. E. Dowling, and W. B. McKinnon, pp. 457–483, Cambridge Univ. Press, Cambridge, U. K.

Moore, C. H., D. B. Goldstein, P. L. Varghese, L. M. Trafton, and B. Stewart (2009), 1-D DSMC simulation of Io's atmospheric collapse and reformation during and after eclipse, *Icarus*, *201*, 585–597, doi:10.1016/j.icarus.2009.01.006.

Morgan, T. H., A. E. Potter, J. B. Corliss, R. M. Killen, F. Scherb, and R. C. Woodward (2004), Post-eclipse growth of Io's sodium emissions, American Astronomical Society, DPS meeting #36, #16.05; Bulletin of the American Astronomical Society, Vol. 36, p.1099.

Moses, J. I., M. Y. Zolotov, and B. Fegley (2002), Alkali and chlorine photochemistry in a volcanically driven atmosphere at Io, *Icarus*, *156*, 107–135, doi:10.1006/icar.2001.6759.

Moullet, A., M. A. Gurwell, E. Lellouch, and R. Moreno (2010), Simultaneous mapping of SO_2, SO, NaCl in Io's atmosphere with the Submillimeter Array, *Icarus*, *208*(1), 353–365, doi:10.1016/j.icarus.2010.02.009.

Moullet, A., E. Lellouch, R. Moreno, M. Gurwell, J. H. Black, and B. Butler (2013), Exploring Io's atmospheric composition with APEX: First measurement of 34SO2 and tentative detection of KCl, *Astrophys. J.*, *776*(1), 32, doi:10.1088/0004-637X/776/1/32.

Nelson, R. M. (1977), Search for color changes and brightening of Io upon eclipse reappearance, *Icarus*, *32*, 225–228, doi:10.1016/0019-1035(77)90061-6.

Nelson, R. M., and B. W. Hapke (1978), Possible correlation of Io's posteclipse brightening with major solar flares, *Icarus*, *33*, 203–209, doi:10.1016/0019-1035(78)90033-7.

Nelson, R. M., A. L. Lane, M. E. Morrill, B. D. Wallis, J. Gibson, W. D. Smythe, L. J. Horn, and B. J. Buratti (1993), The brightness of Jupiter's satellite Io following emergence from eclipse—Selected observations, 1981–1989, *Icarus*, *101*(2), 223–233, doi:10.1006/icar.1993.1020.

Pearl, J., R. Hanel, V. Kunde, W. Maguire, K. Fox, S. Gupta, C. Ponnamperuma, and F. Raulin (1979), Identification of gaseous SO_2 and new upper limits for other gases on Io, *Nature*, *280*, 755–758, doi:10.1038/280755a0.

Retherford, K. D., et al. (2007), Io's atmospheric response to eclipse: UV aurorae observations, *Science*, *318*, 237–240, doi:10.1126/science.1147594.

Roth, L., J. Saur, K. D. Retherford, D. F. Strobel, and J. Spencer (2011), Simulation of Io's auroral emission: Constraints on the atmosphere in eclipse, *Icarus*, *214*(2), 495–509, doi:10.1016/j.icarus.2011.05.014.

Saur, J., F. M. Neubauer, D. F. Strobel, and M. E. Summers (1999), Three-dimensional plasma simulation of Io's interaction with the Io plasma torus: Asymmetric plasma flow, *J. Geophys. Res.*, *104*(A11), 25,105–25,126, doi:10.1029/1999JA900304.

Schaefer, L., and B. Fegley (2005), Alkali and halogen chemistry in volcanic gases on Io, *Icarus*, *173*(2), 454–468, doi:10.1016/j.icarus.2004.08.015.

Schneider, N. M., and F. Bagenal (2007), Io's neutral clouds, plasma torus, and magnetospheric interaction, in "*Io After Galileo: A New View of Jupiter's Volcanic Moon*", edited by R. M. C. Lopes and J. R. Spencer, pp. 265, Published by Springer Praxis Books/Geophysical Sciences, Part of Springer Science + Business Media, Berlin, Germany, 2007, doi: 10.1007/978-3-540-48841-5_11.

Schneider, N. M., D. M. Hunten, W. K. Wells, A. B. Schultz, and U. Fink (1991a), The structure of Io's corona, *Astrophys. J. Part 1*, *368*, 298–315, doi:10.1086/169694.

Schneider, N. M., J. K. Wilson, J. T. Trauger, D. I. Brown, R. W. Evans, and D. E. Shemansky (1991b), Molecular origin of Io's fast sodium, *Science*, *253*, 1394–1397, doi:10.1126/science.253.5026.1394.

Spencer, J. R., J. A. Rathbun, L. D. Travis, L. K. Tamppari, L. Barnard, T. Z. Martin, and A. S. McEwen (2000), Io's thermal emission from the Galileo photopolarimeter-radiometer, *Science*, *288*, 1198–1201, doi:10.1126/science.288.5469.1198.

Spencer, J. R., K. L. Jessup, C. C. C. Tsang, N. Cunningham, and K. Retherford (2012), Evidence for volcanic support of Io's Jupiter-facing atmosphere from constraints on post-eclipse atmospheric changes, 43rd Lunar and Planetary Science Conference, held March 19–23, 2012 at The Woodlands, Texas. LPI Contribution No. 1659, id.2420.

Summers, M. E., and D. F. Strobel (1996), Photochemistry and vertical transport in Io's atmosphere and ionosphere, *Icarus*, *120*, 290–316, doi:10.1006/icar.1996.0051.

Trafton, L. (1975), Detection of a potassium cloud near Io, *Nature*, *258*, 690–692, doi:10.1038/258690a0.

Trafton, L., T. Parkinson, and W. Macy Jr. (1974), The spatial extent of sodium emission around Io, *Astrophys. J.*, *190*, L85–L89.

Trafton, L. M., C. H. Moore, D. B. Goldstein, P. L. Varghese, and M. A. McGrath (2012), HST/STIS observations and simulation of Io's emission spectrum in Jupiter shadow: Probing Io's Jupiter-facing eclipse atmosphere, *Icarus*, *220*(2), 1121–1140, doi:10.1016/j.icarus.2012.06.025.

Tsang, C. C., J. R. Spencer, E. Lellouch, M. A. López-Valverde, M. J. Richter, and T. K. Greathouse (2012), Io's atmosphere: Constraints on sublimation support from density variations on seasonal timescales using NASA IRTF/TEXES observations from 2001 to 2010, *Icarus*, *217*(1), 277–296, doi:10.1016/j.icarus.2011.11.005.

Tsang, C. C., J. R. Spencer, E. Lellouch, M. A. López-Valverde, M. J. Richter, and T. K. Greathouse (2013), Io's contracting atmosphere post 2011 perihelion: Further evidence for partial sublimation support on the anti-Jupiter hemisphere, *Icarus*, *226*(1), 1177–1181, doi:10.1016/j.icarus.2013.06.032.

Walker, A. C., C. H. Moore, D. B. Goldstein, P. L. Varghese, and L. M. Trafton (2012), A parametric study of Io's thermophysical surface properties and subsequent numerical atmospheric simulations based on the best fit parameters, *Icarus*, *220*, 225–253, doi:10.1016/j.icarus.2012.05.001.

Wilson, J. K., and N. M. Schneider (1999), Io's sodium directional feature: Evidence for ionospheric escape, *J. Geophys. Res.*, *104*(E7), 16,567–16,584, doi:10.1029/1999JE900017.

Wilson, J. K., M. Mendillo, J. Baumgardner, N. M. Schneider, J. T. Trauger, and B. Flynn (2002), The dual sources of Io's sodium clouds, *Icarus*, *157*(2), 476–489, doi:10.1006/icar.2002.6821.

Wolven, B. C., H. W. Moos, K. D. Retherford, P. D. Feldman, D. F. Strobel, W. H. Smyth, and F. Roesler (2001), Emission profiles of neutral oxygen and sulfur in Io's exospheric corona, *J. Geophys. Res.*, *106*(A11), 26,155–26,182, doi:10.1029/2000JA002506.

Wong, M. C., and W. H. Smyth (2000), Model calculations for Io's atmosphere at eastern and western elongations, *Icarus*, *146*(1), 60–74, doi:10.1006/icar.2000.6362.

Yoneda, M., M. Kagitani, and S. Okano (2009), Short-term variability of Jupiter's extended sodium nebula, *Icarus*, *204*(2), 589–596, doi:10.1016/j.icarus.2009.07.023.

Yoneda, M., F. Tsuchiya, H. Misawa, B. Bonfond, C. Tao, M. Kagitani, and S. Okano (2013), Io's volcanism controls Jupiter's radio emissions, *Geophys. Res. Lett.*, *40*, 671–675, doi:10.1002/grl.50095.